AIP | Review of Scientific Instruments

Practical guide for validated memristance measurements

Nan Du, Yao Shuai, Wenbo Luo, Christian Mayr, René Schüffny, Oliver G. Schmidt, and Heidemarie Schmidt

Citation: Review of Scientific Instruments **84**, 023903 (2013); doi: 10.1063/1.4775718
View online: http://dx.doi.org/10.1063/1.4775718
View Table of Contents: http://scitation.aip.org/content/aip/journal/rsi/84/2?ver=pdfcov
Published by the AIP Publishing

Articles you may be interested in

Novel implementation of memristive systems for data encryption and obfuscation
J. Appl. Phys. **115**, 124501 (2014); 10.1063/1.4869262

Spin transport in memristive devices
Appl. Phys. Lett. **100**, 043510 (2012); 10.1063/1.3679114

Memristive adaptive filters
Appl. Phys. Lett. **97**, 093502 (2010); 10.1063/1.3485060

A magnetron sputtering system for the preparation of patterned thin films and in situ thin film electrical resistance measurements
Rev. Sci. Instrum. **78**, 103901 (2007); 10.1063/1.2793508

A cool(ing) idea
Phys. Teach. **36**, 512 (1998); 10.1119/1.879943

Edwards are at the forefront of vacuum technology for R&D and lab applications.
Click here for product information

This article is copyrighted as indicated in the article. Reuse of AIP content is subject to the terms at: http://scitationnew.aip.org/termsconditions. Downloaded to IP: 130.60.6.54 On: Tue, 13 May 2014 07:16:36

REVIEW OF SCIENTIFIC INSTRUMENTS **84**, 023903 (2013)

Practical guide for validated memristance measurements

Nan Du,[1,2,a)] Yao Shuai,[3] Wenbo Luo,[3] Christian Mayr,[4] René Schüffny,[4]
Oliver G. Schmidt,[1,2] and Heidemarie Schmidt[1]
[1]*Faculty of Electrical Engineering and Information Technology, University of Technology Chemnitz, 09107 Chemnitz, Germany*
[2]*Institute for Integrative Nanosciences, IFW Dresden, Helmholtzstraße 20, 01069 Dresden, Germany*
[3]*Helmholtz Research Center Dresden-Rossendorf e.V., Bautzner Landstrasse 400, 01328 Dresden, Germany*
[4]*Department of Electrical Engineering and Information Technology, University of Technology Dresden, Helmholtz Str. 18, 01062 Dresden, Germany*

(Received 15 August 2012; accepted 26 December 2012; published online 13 February 2013)

Chua [IEEE Trans. Circuit Theory **18**, 507–519 (1971)] predicted rather simple charge-flux curves for active and passive memristors (short for memory resistors) and presented active memristor circuit realizations already in the 1970 s. The first passive memristor has been presented in 2008 [D. B. Strukov, G. S. Snider, and D. R. Williams, Nature (London) **453**, 80–83 (2008)]. Typically, memristors are traced in complicated hysteretic current-voltage curves. Therefore, the true essence of many new memristive devices has not been discovered so far. Here, we give a practical guide on how to use normalized charge-flux curves for the prediction of hysteretic current-voltage characteristics of memristors. In the case of memristive $BiFeO_3$ thin film capacitor structures, the normalized charge-flux curves superimpose for different numbers of measurement points N_s and a different measurement time per measurement point T_s. Such normalized charge-flux curves can be used for the prediction of current-voltage characteristics for input signals with arbitrarily chosen N_s and T_s. © *2013 American Institute of Physics*. [http://dx.doi.org/10.1063/1.4775718]

I. INTRODUCTION

Hysteretic current-voltage behavior can be observed in nanoscale two-terminal electronic devices, which involve the motion of charged atoms or molecules. In 2008, Strukov *et al.*[2] showed that certain titanium dioxide cross-point nanostructures reveal hysteretic current-voltage behavior and presented a physical model which connected the ohmic electronic conduction and linear ionic drift with the memristance of the titanium dioxide nanostructures. Since this seminal work nonvolatile bistable hysteretic current-voltage behavior has been observed in many nanoscale two-terminal devices, e.g., in graphene-copper oxide-copper microjunctions,[3] in gold-bismuth iron oxide-platinum junctions,[4] in silver-amorphous silicon-*p*-type silicon nanojunctions,[5] and in two serial platinum-silicon oxide/germanium selenide-copper nanojunctions,[6] just to mention few of them. Volatile bistable hysteretic current-voltage behavior has been reported very frequently, e.g., in silver epoxy-vanadium dioxide-silver epoxy microjunctions.[7] Chua[1] presented an electromagnetic field interpretation of such two-terminal devices which relates charge and flux (q-φ). He labeled this so far undefined circuit element memristor and theoretically showed that almost any (q-φ) curve can be generated in practice by active networks.[1] The voltage across a charge-controlled memristor is given by the incremental memristance $M(q)$

$$M(q) = \frac{d\varphi}{dq}. \quad (1)$$

The current of a flux-controlled memristor is given by the incremental memconductance $W(\varphi)$

$$W(\varphi) = \frac{dq}{d\varphi}. \quad (2)$$

In a very special case where the (q-φ) curve is a straight line, the memristor reduces to a linear-time invariant resistor with resistance R and it holds that

$$M(q) = \frac{1}{W(\varphi)} = R. \quad (3)$$

Memristors range from binary to multi-state memories and can be used for signal processing for waveform generators and for neuromorphic architectures. For memristor devices to become reality, a deeper understanding of the memristor's dynamic nature is necessary.[8] For example, in ZnO nano- and microwires, the hysteretic current-voltage behavior has been observed from 100 Hz to 10 kHz. At 10 Hz and below the current-voltage curve was linear.[12] Our analysis is specifically targeting key electrical memristor device characteristics relevant to memory operations. Ho *et al.*[9] investigated the design of read and write circuits for nonvolatile memristor memories and analyzed important data integrity and noise-tolerance issues. The memristor used is an electrically switchable TiO_2 thin film sandwiched between two metal contacts with well-defined charge-controlled memristance $M(q)$ and flux-controlled memristance $M(\varphi)$. Here, $M(q)$ and $M(\varphi)$ depend on the distance D between the two metal contacts and on the width w and width (D-w) of the doped and undoped TiO_2 region, respectively. The constraint is given by $0 \le w \le D$.[2]

Rajendran *et al.*[10] used the unique relationship between charge and flux in switchable TiO_2 thin films[2] to design memristors for neuromorphic computing, memory, and field

a)Author to whom correspondence should be addressed. Electronic mail: Nan.Du@s2012.tu-chemnitz.de.

 © 2013 American Institute of Physics

This article is copyrighted as indicated in the article. Reuse of AIP content is subject to the terms at: http://scitationnew.aip.org/termsconditions. Downloaded to IP: 130.60.6.54 On: Tue, 13 May 2014 07:16:36

programmable gate array applications. There are only few reports on modeling memristance of memristive materials other than switchable TiO_2 thin films. Ukil[11] has derived an expression for the charge-controlled memristance $M(q)$ of memristive piezoelectric materials and found a relationship between $M(q)$ and the distance between the two contacts attached to the piezoelectric material, its cross-sectional area, and resistivity. The first step in the design flow of new memristive devices is to accurately model the memristor device.[13–15] As discussed above memristor devices have been modeled using the linear drift velocity model proposed in Ref. 2. We are not aware of charge-controlled $M(q)$ or flux-controlled $M(\varphi)$ data of many other memristive materials, e.g., of those revealing nonvolatile bistable resistance states[3–6] or volatile resistance states.[7]

In this paper, we present a practical guide for validated memristance measurements on memristive materials with unknown charge-controlled $M(q)$ or flux-controlled $M(\varphi)$ data. Besides strictly using the well-known relationships between charge q and current i

$$q(t) = \int_{-\infty}^{t} i(\tau)\mathrm{d}\tau, \tag{4}$$

and between flux φ and voltage v

$$\varphi(t) = \int_{-\infty}^{t} v(\tau)\mathrm{d}\tau, \tag{5}$$

we reveal the dependence of $M(q)$ and $M(\varphi)$ on the time-dependent current and voltage, respectively. Furthermore, we point out the difference of clockwise (CW) and counterclockwise (CCW) cycled $M(q)$ and $M(\varphi)$ data and establish comparability between differently recorded (q-φ) data by introducing a normalization point at the CW and CCW turning point. Finally, the (q-φ) data are used to predict hysteretic current-voltage characteristics of linear time-invariant resistors and of gold-bismuth iron oxide-platinum junctions[4] for CW and CCW cycled linear, sinusoidal, and exponential current and voltage input signals.

The paper is organized as follows. A sketch of the experimental measurement circuitry together with the data handling scheme is shown in Sec. II. The measured (q-φ) data are represented and their normalization is discussed in Sec. III. In Sec. IV, (q-φ) data are used to calculate (i-v) data of linear time-invariant resistors and of nonlinear time-dependent resistors, and the calculated and measured (i-v) data for comparable CW and CCW cycled linear, sinusoidal, and exponential current and voltage input signals are compared. The paper closes with Sec. V.

II. DATA RECORDING AND ANALYSIS

While it is usually no problem to collect (i-v) data of linear time-invariant resistors without memory in voltage correct measurements and in current correct measurements, some possible pitfalls have to be considered when collecting hysteretic (i-v) data of memristors. In the following, a memristance measurement setup will be presented (Fig. 1). We recommend a manual range selection for the input voltage $v_{in}(t)$ in voltage correct measurements. The corresponding output

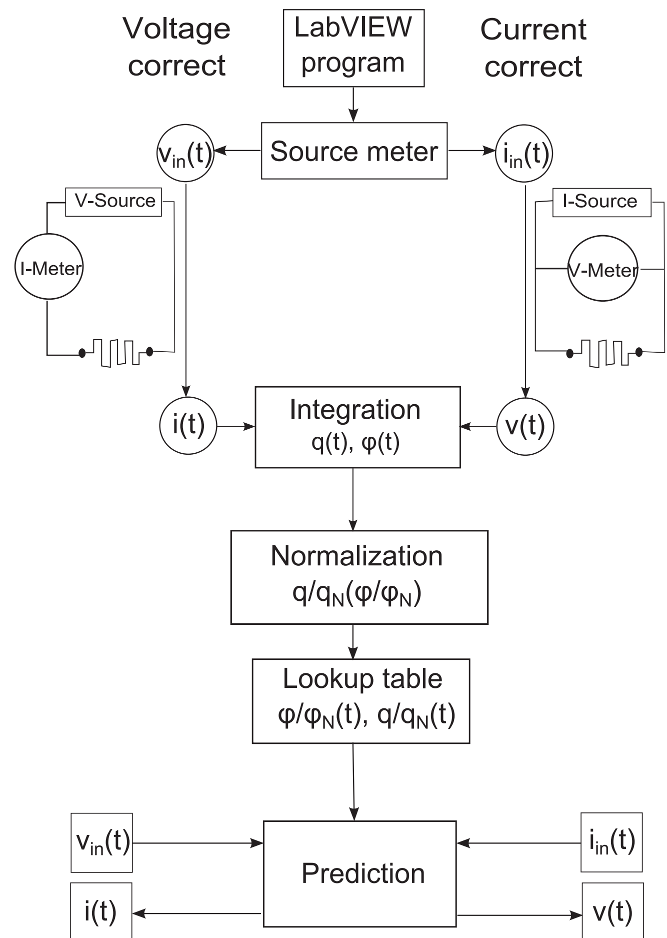

FIG. 1. Combined block diagram of the memristance measurement setup and flow chart of validated memristance measurements. The experimental setup uses a Keithley source meter to define the input voltage $v_{in}(t)$ or the input current $i_{in}(t)$ with respect to its amplitude V_{dc} and I_{dc} and to its shape, e.g., linear, exponential, or sinusoidal, to its number of measurement points N_s and to the measurement time T_s per measurement point for voltage correct (left) and for current correct (right) measurements. The measurement is controlled by a LabVIEW program. This program also collects the output current $i(t)$ (left) and output voltage $v(t)$ (right) data, performs the integration according to Eqs. (4) and (5) and the normalization according to Eqs. (6) and (7), stores the normalized memristance data in a lookup table and predicts (i-v) curves from normalized memristance curves for input voltage v_{in} (left) and input current i_{in} (right) with corresponding shape and amplitude and arbitrarily chosen N_s and T_s.

current $i(t)$ data may be used to select the range for the input current $i_{in}(t)$ in current correct measurements. We recommend to source the CW and CCW cycles always from the origin. If other source points will be used as a starting point, minor loops of the hysteretic (i-v) data will be probed. The (i-v) data collection has to be repeated several times in order to check stability of the hysteretic (i-v) data. For stable hysteretic (i-v) data and well-defined initial states of the memristor, an increase in the number of collected (i-v) data is recommendable. This may be reached by increasing the number of measurement points N_s. Finally, the validity of normalized (q-φ) data may be checked by comparing normalized (q-φ) data where the corresponding unnormalized (q-φ) data have been recorded with different measurement time T_s per measurement point.

This article is copyrighted as indicated in the article. Reuse of AIP content is subject to the terms at: http://scitationnew.aip.org/termsconditions. Downloaded to IP: 130.60.6.54 On: Tue, 13 May 2014 07:16:36

III. EXPERIMENTAL RESULTS

A. Input signal

First, we checked validated memristance measurements on linear time-dependent 100 Ω and 200 Ω resistors. Figure 2 shows the charge q as a function of the corresponding flux through the sample for both CW (1st quadrant) and CCW (3rd quadrant) voltage (Fig. 2(a)) and current (Fig. 2(b)) sweep, respectively. The sinusoidal, linear, and exponential input voltage has an amplitude V_{dc} of 7 V. As illustrated in Fig. 2, the (q-φ) data in CW and CCW directions are symmetric about the origin and the coordinates of the turning points B_{CW} and B_{CCW} change with the shape of the input signal. The (q-φ) slope (Eq. (2)) is only dependent on the resistance R of the 100 Ω and 200 Ω resistors (Eq. (3)) and not on the shape of input signals.

The input voltage v_{in} has been manually selected and the output current $i(t)$ has been used to select the input current $i_{in}(t)$ in current correct measurements. Figure 2(b) shows the charge-flux curve of the same 100 Ω and 200 Ω resistors from current correct measurement. For the selected input voltage $v_{in}(t)$ (Fig. 2(a)) and input current $i_{in}(t)$ (Fig. 2(b)), the turning points B_{CW} and B_{CCW} are the same. After testing the influence of the shape of input current for the very special case of linear time-independent resistors, validated memristance measurements of a memristor with memory will be checked. For that we have chosen a Au/$BiFeO_3$ (BFO)/Pt thin film capacitor structure.[2] The circular Au top contacts have an area of 8.92 × 10^{-2} mm^2. The (i-v) data collection on BFO can be repeated several times without changing the hysteretic (i-v) characteristics. Furthermore, a nonvolatile low resistance state (LRS) and high resistance state (HRS) can be written in BFO by applying a writing pulse of +9 V and −9 V, respectively.[2] The range for the input voltage v_{in} in voltage correct measurements (Fig. 3(a)) has been selected manually so that breakthrough of the Au/BFO/Pt thin film capacitor structure during looping is avoided. The corresponding output current $i(t)$ has been used to select the range for the input current i_{in} in current correct measurements (Fig. 3(b)).

The CW and CCW forward bias (Fig. 3(a)) is defined as a looping input signal applied to the Au top contact. The voltage sequence during CW looping is: 0 V → 7 V

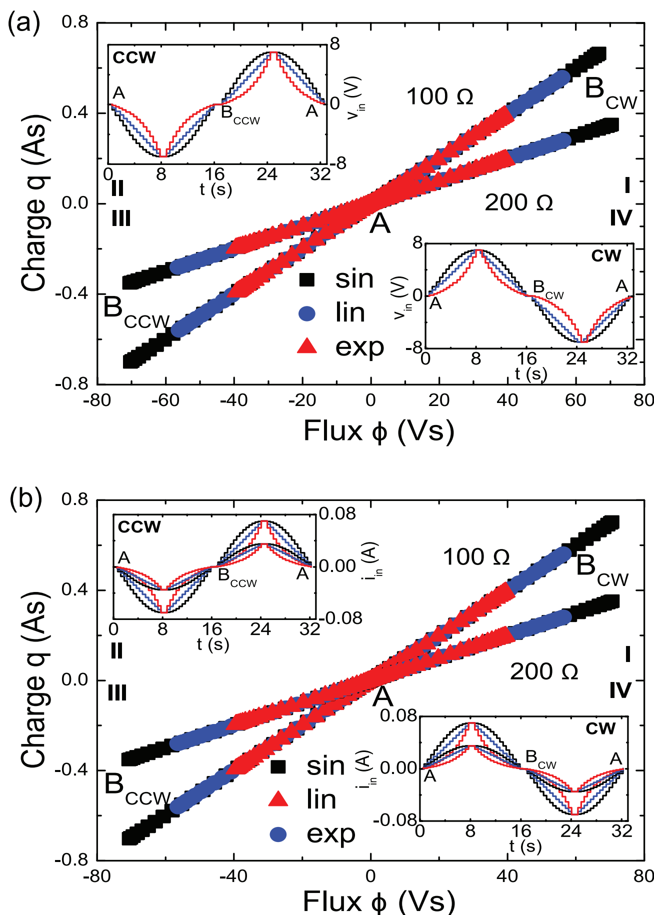

FIG. 2. Charge-flux (q-φ) curve from a 100 Ω and 200 Ω resistor. The insets show the linear (lin), sinusoidal (sin), and exponential (exp) (a) input voltage v_{in} (32 s period T, 7 V amplitude V_{dc}) and (b) input current i_{in} (32 s period T, 70 mA amplitude I_{dc} for 100 Ω and 35 mA amplitude I_{dc} for 200 Ω) for CW and CCW looping. The number of measurement points in each period amounts to $N_s = 64$ and the measurement time T_s per measurement point amounts to $T_s = 0.5$ s. The (q-φ) curve from a resistor lies in the 1st quadrant (I) and in the 3rd quadrant (III), if the input signals are looped CW and CCW, respectively.

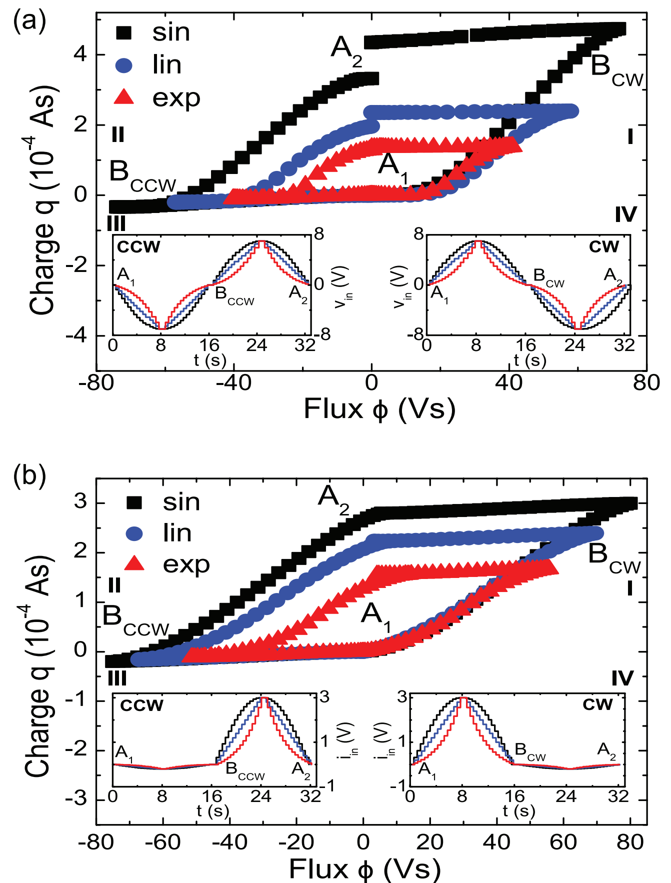

FIG. 3. (a) and (b) Unnormalized charge-flux curves from a BFO memristor with a nominal top contact area of 8.92 × 10^{-2} mm^2. The insets show the sinusoidal (sin), linear (lin), and exponential (exp) (a) input voltage v_{in} (32 s period T, 7 V amplitude V_{dc}) and (b) input current i_{in} (32 s period T, +3 × 10^{-5} A maximum positive input current and −2 × 10^{-6} A minimum negative input current). The number of measurement points in each CW and CCW cycle amounts to $N_s = 64$ and the measurement time T_s per measurement point amounts to $T_s = 0.5$ s.

This article is copyrighted as indicated in the article. Reuse of AIP content is subject to the terms at: http://scitationnew.aip.org/termsconditions. Downloaded to IP: 130.60.6.54 On: Tue, 13 May 2014 07:16:36

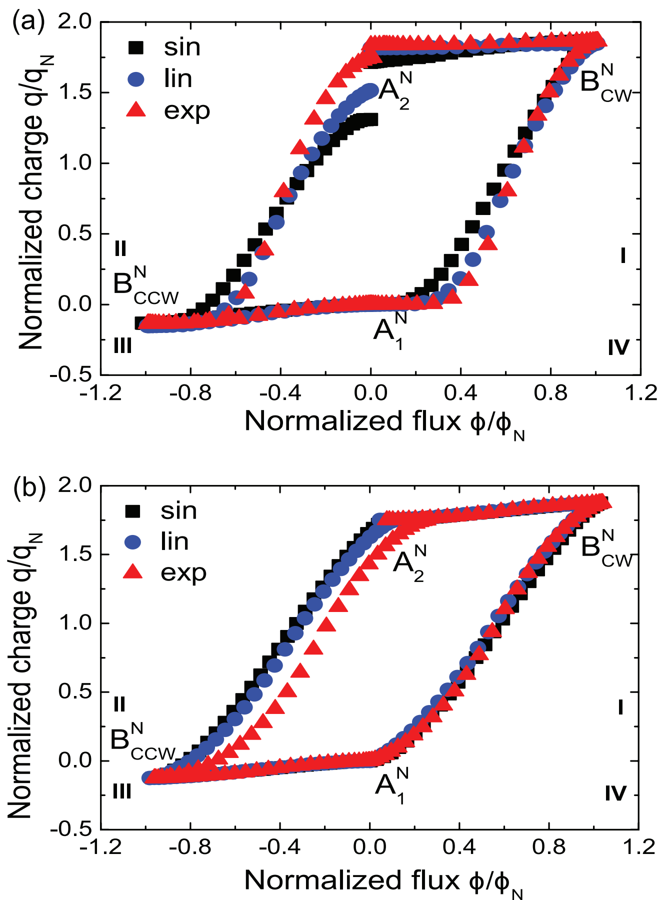

FIG. 4. Normalized charge-flux curves from the BFO memristor in Fig. 3 for (a) input voltage and (b) input current. The number of measurement points in each CW and CCW cycle amounts to $N_s = 64$ and the step length amounts to $T_s = 0.5$ s. The turning points of the normalized CW and CCW memristance curve lie at $B^N_{\text{CW}} = (1, 1.89)$ and $B^N_{\text{CCW}} = (-1, -0.18)$, respectively.

→ −7 V → 0 V and the voltage sequence for CCW looping is: 0 V → −7 V → 7 V → 0 V. The memristance data lie in the I and II-III quadrant for clockwise and counterclockwise cycling of the input voltage, respectively. Therefore, Au/BFO/Pt thin film capacitor structures are partially active, have a storage capacity and are no ideal memristors.

The homogeneous and stable performance is revealed by measuring sinusoidal, linear, and exponential input voltage (Fig. 3(a)) and input current (Fig. 4(3)). By applying a positive voltage the pristine BFO sample can be switched to LRS, while the HRS is reset by a negative voltage. The resistance ratio between the HRS and LRS is more than two orders of magnitude at a reading voltage of +2 V.

B. Normalized memristance

As has been shown in Sec. II the (q-φ) curve depends on the shape, amplitude, number of measurement points N_s, and time per measurement point T_s of the input signal.

In the following, we will introduce normalized (q-φ) curves which will allow to predict the current-voltage behavior for input signals of the same shape and amplitude in different frequency ranges, i.e., with different N_s and T_s. For a given shape and amplitude of the input signal the absolute values of the coordinates of the B_{CW} and B_{CCW} turning points, φ^{CW}, q^{CW}, φ^{CCW}, and q^{CCW}, increase with increasing number of measurement points N_s and with increasing measurement time per measurement point. For normalization we use the coordinates of the turning points $B_{\text{CW}} = B_{\text{CW}}(\varphi^{\text{CW}}, q^{\text{CW}})$ and $B_{\text{CCW}} = B_{\text{CCW}}(\varphi^{\text{CCW}}, q^{\text{CCW}})$. The normalization factor q_N for charge is given by

$$q_N = (|q^{CW}| + |q^{CCW}|)/2 \tag{6}$$

and the normalization factor φ_N for flux is given by

$$\varphi_N = (|\varphi^{\text{CW}}| + |\varphi^{\text{CCW}}|)/2. \tag{7}$$

For resistors it holds that $q_N = |q^{\text{CW}}| = |q^{\text{CCW}}|$ and $\varphi_N = |\varphi^{\text{CW}}| = |\varphi^{\text{CCW}}|$. Therefore, the normalization factors can be obtained from CW or CCW cycled signals. Memristance data are normalized by dividing φ by φ_N and q by q_N. The turning points of normalized memristance curves are labeled B^N_{CW} and B^N_{CCW}. For resistors with resistance R it follows

$$R = \frac{\varphi_N}{q_N}. \tag{8}$$

Therefore, for normalized memristance information on the normalization factors φ_N and q_N is needed. As will be shown in the following, for normalized memristance curves of memristors additional information on the shape and amplitude of the input signal will be needed.

The memristance curves for different CW and CCW input voltage (Fig. 4(a)) and input current (Fig. 4(b)) measurements have been normalized using the normalization factors q_N and φ_N from Eqs. (6) and (7). The normalized turning points B^N_{CW} and B^N_{CCW} have been calculated. For memristors, it holds that $q_N \neq |q^{\text{CW}}| \neq |q^{\text{CCW}}|$ and $\varphi_N \neq |\varphi^{\text{CW}}| \neq |\varphi^{\text{CCW}}|$. Therefore, the normalization factors of memristors can only be obtained from both CW and CCW cycled signals. For example, for sinusoidal, linear, and exponential CW input voltage (Fig. 4(a)), the normalized turning point $B^N_{\text{CW}}(\varphi^{\text{CW}}/\varphi_N, q^{CW}/q_N)$ lies at (1, 1.89). In comparison to the coordinate values of the normalized CW turning point of resistors, the coordinate values of the normalized CW turning point of memristors range from 0 to 2.

IV. MODELING OF HYSTERETIC (I-V) DATA

In the following, it is demonstrated how to predict hysteretic (i-v) data of memristive materials for an arbitrarily chosen number of measurement points N_s and measurement time per measurement point T_s. We use the fact that the normalized memristance curves superimpose for arbitrarily chosen N_s and T_s. As the first example we start from normalized memristance curves of the BFO memristor which have been obtained by validated memristance measurements for a CW 7 V input voltage of different shape. They can be saved in lookup tables together with information on the amplitude and shape of the input signal (Fig. 1). The normalized memristance curves (Fig. 5(a)) depend on the shape of the CW 7 V input voltage (Fig. 5(a)). Mainly in the q/q_N range from 0 to 0.8 the shape of the input voltage strongly influences the normalized memristance data. Next, we chose an input signal of the same shape and amplitude as the input signals

This article is copyrighted as indicated in the article. Reuse of AIP content is subject to the terms at: http://scitationnew.aip.org/termsconditions. Downloaded to IP: 130.60.6.54 On: Tue, 13 May 2014 07:16:36

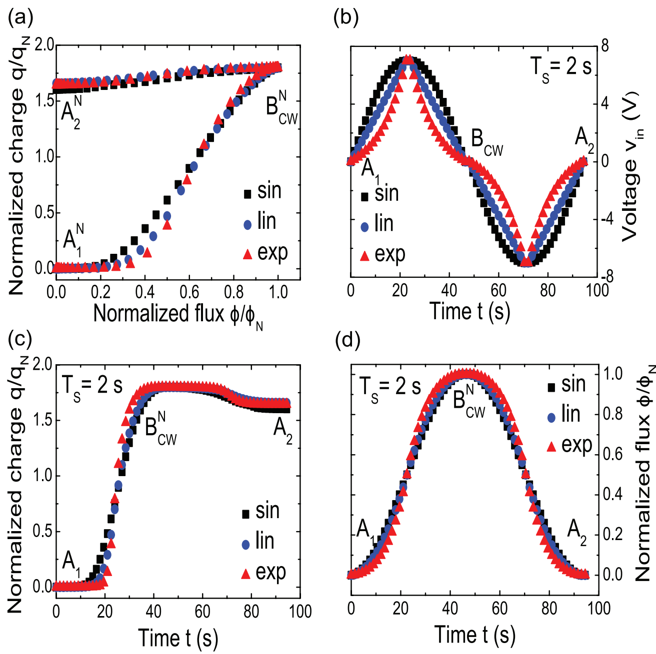

FIG. 5. (a) Normalized memristance curve in the first (I) quadrant from a BFO memristor with a nominal top contact area of 8.92 × 10^{-2} mm^2 recorded with CW 7 V input voltage v_{in} of different shape. The turning point lies at $B^N_{\mathrm{CW}} = (1, 1.798)$. (b) Sinusoidal (sin), linear (lin), and exponential (exp) input voltage v_{in} (64 measurement steps N_s, 32 ms period T, 7 V amplitude V_{dc}, measurement time $T_s = 2$ s). (c) Normalized charge curves and (d) normalized flux curves for the input voltage v_{in} represented in (b).

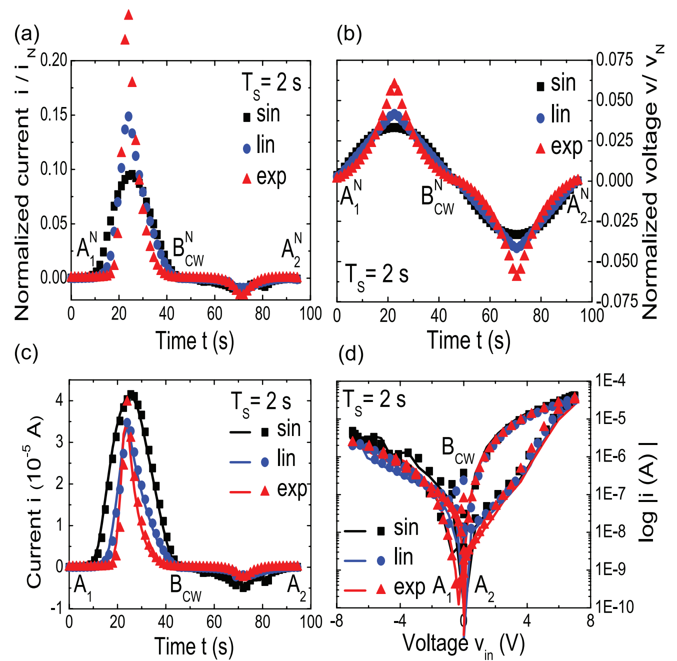

FIG. 6. (a) Normalized current curves obtained by differentiating the normalized charge curve (Fig. 5(c)) recorded on a BFO memristor with a CW input voltage v_{in} of different shape and with the same amplitude. (b) Normalized input voltage curves obtained by differentiating the normalized flux curve (Fig. 5(d)). Predicted (solid lines) and experimental (symbols) unnormalized output current (c) versus time on a linear scale and (d) versus input voltage on a logarithmic scale.

used for validated memristance data (Fig. 5(a)), but with an arbitrarily chosen number of measurement points N_s and an arbitrarily chosen measurement time per measurement point T_s. As an example, a sinusoidal, linear, and exponential input voltage v_{in} with $N_s = 64$ and $T_s = 2$ s has been chosen (Fig. 5(b)). Using Eq. (5) and the normalization factor φ_N (Eq. (7)) we calculate the normalized flux $\varphi(t)/\varphi_N$ (Fig. 5(d)) from the input voltage (Fig. 5(b)). From the normalized memristance data (Fig. 5(a)) or from the data in the corresponding lookup table $(\varphi(t)/\varphi_N, q(t)/q_N)$ we determine the normalized charge $q(t)/q_N$ (Fig. 5(c)).

From the derivative of the normalized charge curve (Fig. 5(c)) and of the normalized flux curve (Fig. 5(d)), we obtain the normalized current curve (Fig. 6(a)) and the normalized voltage curve (Fig. 6(b)), respectively. Finally, we multiply the normalized current curve with the normalization factor q_N and the normalized flux curve with the normalization factor φ_N and obtain the output current $i(t)$ (Fig. 6(c)) for an input voltage with arbitrarily chosen N_s and T_s. For a better comparison with experiment the output current $i(t)$ can also be plotted versus the input voltage $v_{in}(t)$. The calculated $(i\text{-}v)$ data (solid lines) are shown together with experimental data (symbols) on a logarithmic scale (Fig. 6(d)). Tiny features of the $(i\text{-}v)$ data are very well reproduced and prove the validity of the presented concept. As a second example, we demonstrate how memristance curves for input signals of a given shape and amplitude can be used to predict hysteretic $(i\text{-}v)$ data of memristive materials for input signals of the same shape and amplitude and arbitrarily chosen measurement time per measurement point T_s. We start from the normalized memristance curve (Fig. 7(a)) which has been recorded with a CW 7 V linear input voltage by validated memristance measurements as described in Sec. II (Fig. 1). The arbitrarily chosen measurement times per measurement point T_s are 0.5 s, 1 s, and 2 s. Since the normalized memristance curves superimpose for the different T_s, we can predict the $(i\text{-}v)$ data from the normalized memristance (Fig. 7(a)) for arbitrarily chosen measurement times per measurement point T_s. The normalization factor φ_N depends on T_s and is calculated from the CW linear input voltage v_{in} (Fig. 7(b)). The corresponding normalization factor q_N is proportional with φ_N and determined from the turning point B^N_{CW} in the normalized memristance (Fig. 7(a)). The calculated $(i\text{-}v)$ data (solid lines) have been plotted together with experimental data (symbols) on a linear scale (Fig. 7(c)) and on a logarithmic scale (Fig. 7(d)). The maximum positive current and minimum negative current strongly depend on T_s and are largest for the largest T_s (Fig. 7(c)). Mainly for negative input voltage it is obvious that all tiny features of the $(i\text{-}v)$ data are very well reproduced.

As a third example, we demonstrate how for input signals of given shape and different amplitude the normalized memristance curves can be used to recover hysteretic $(i\text{-}v)$ data. Note that input signals with different amplitudes allow for an investigation of minor-loop hysteretic $(i\text{-}v)$ data. For a better comparison the number of measurement points N_s and the measurement time per measurement point T_s have been kept fixed. We start from the normalized memristance curve (Fig. 8(a)) which has been obtained by validated memristance measurements (Fig. 1). Here, we chose a CW linear input voltage v_{in} with three different amplitudes of 7 V, 5 V, and

This article is copyrighted as indicated in the article. Reuse of AIP content is subject to the terms at: http://scitationnew.aip.org/termsconditions. Downloaded to IP: 130.60.6.54 On: Tue, 13 May 2014 07:16:36

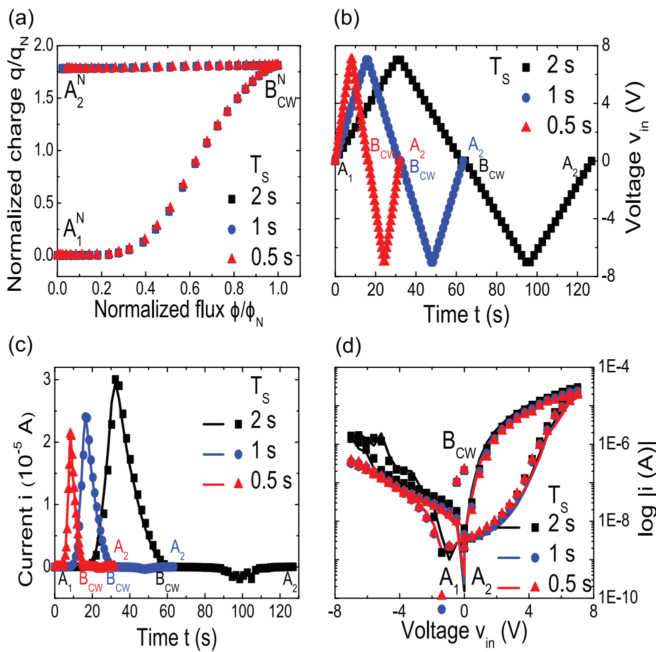

FIG. 7. (a) Normalized memristance curve from a BFO memristor with a nominal top contact area of 8.92×10^{-2} mm^2 recorded with a CW linear (lin) input voltage v_{in} of the same shape and amplitude and different measurement time per measurement point $T_s = 0.5$, 1, 2 s. The turning point lies at $B_{\mathrm{CW}}^{N} = (1, 1.81)$. (b) Linear (lin) input voltage v_{in} (64 measurement steps N_s, 7 V amplitude V_{dc}, 0.5, 1, and 2 s measurement time T_s). Predicted (solid lines) and experimental (symbols) unnormalized output current (c) versus time on a linear scale and (d) versus input voltage on a logarithmic scale.

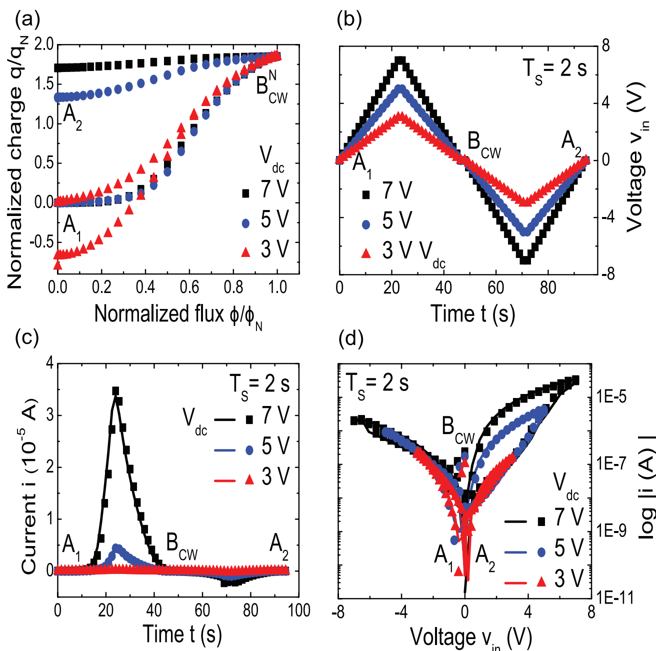

FIG. 8. (a) Normalized memristance curve from a BFO memristor with a nominal top contact area of 8.92×10^{-2} mm^2 recorded with a CW input voltage v_{in} of the same shape and of different amplitude. The turning point of the normalized CW curves of the memristor lies at $B_{\mathrm{CW}}^{N} = (1, 1.85)$. (b) Linear (lin) input voltage v_{in} with different amplitude (64 measurement steps N_s, 32 s period T, measurement time $T_s = 2$ s). Predicted (solid lines) and experimental (symbols) unnormalized output current (c) versus time on a linear scale and (d) versus input voltage v_{in} on a logarithmic scale.

3 V and with a fixed $N_s = 64$ and $T_s = 2$ s (Fig. 8(b)). Normalized memristance data (Fig. 8(a)) depend on the amplitude of the input signal and lie in the 1st and 4th quadrant for a small amplitude of 3 V and in the 1st quadrant only for a large amplitude of 5 V and 7 V. The value of q/q_N is 0.0 at the point A_1 and +1.81 at B_{CW}^{N}. The starting point, half-period point, and full-period point is labeled A_1, B_{CW}, and A_2, respectively. For an amplitude of 3 V, the value of q/q_N at the point A_2 is negative and the hysteresis of the corresponding (i-v) data is small (Fig. 8(a)). Also the maximum positive current and minimum negative current strongly depend on the amplitude of the input voltage and are largest for the largest amplitude (Fig. 8(c)). Here, the normalization factor φ_N depends on the amplitude of the input voltage v_{in}. Again φ_N is calculated from the CW linear input voltage (Fig. 8(b)) and the corresponding normalization factor q_N is determined from the turning point B_{CW}^{N} in the normalized memristance (Fig. 8(a)). Calculated (i-v) data (solid lines) have been plotted together with experimental data (symbols) on a linear scale (Fig. 8(c)) and on a logarithmic scale (Fig. 8(d)). Mainly for positive input voltage it is obvious that all features of the minor-loop hysteretic (i-v) data are well reproduced.

V. CONCLUSIONS AND OUTLOOK

We have presented an experimental setup for charge-flux (q-φ) and for validated memristance measurements. Memristance measurements are useful for the prediction of time-dependent current-voltage characteristics of memristors with stable electrical characteristics in dependence on the shape and amplitude of the input voltage or input current signals. Chua[1] gave an electromagnetic field interpretation of a memristor and predicted rather simple charge-flux curves for active and passive memristors. For voltage or current correct measurements, the input signals are the input voltage or the input current, respectively. The input signal and the correspondingly measured output current and output voltage are integrated and yield charge q and flux φ, respectively. The (q-φ) curves of clockwise (CW) and counterclockwise (CCW) cycled input signals define the turning points B_{CW} and B_{CCW} of the memristance curves, respectively. Unnormalized memristance curves depend on the shape and amplitude of the input signal, the number of measurement points and measurement time per measurement point of the unnormalized input signal. Normalized memristance curves only depend on the shape and amplitude of the input signal and allow for an easier comparison of memristive materials with different dynamic nature. As an example, we have performed validated memristance measurements on memristive thin film Au/BFO/Pt capacitor structures for input signals of different shape and amplitude. The memristance data lie in the I and II-III quadrant for clockwise and counter-clockwise cycling of the input voltage, respectively. Therefore, Au/BFO/Pt structures are partially active and have a storage capacity. In the future, a normalization of memristance curves containing contributions from superimposed harmonic and inharmonic input signals and the normalization of memristance curves from memristors in parallel or in series will be developed.

This article is copyrighted as indicated in the article. Reuse of AIP content is subject to the terms at: http://scitationnew.aip.org/termsconditions. Downloaded to IP: 130.60.6.54 On: Tue, 13 May 2014 07:16:36

ACKNOWLEDGMENTS

H.S. greatly acknowledges financial support from the Deutsche Forschungsgemeinschaft (DFG) (DFGSCHM1663/4-1). N.D. and W.L. acknowledge funding by the Initiative and Networking Fund of the Helmholtz Association (VH-VI-422).

[1] L. O. Chua, IEEE Trans. Circuit Theory **18**, 507–519 (1971).
[2] D. B. Strukov, G. S. Snider, and D. R. Williams, Nature (London) **453**, 80–83 (2008).
[3] S. Kwon, H. Seo, H. Lee, K.-J. Jeon, and J. Y. Park, Appl. Phys. Lett. **100**, 123101 (2012).
[4] Y. Shuai, S. Zhou, D. Bürger, M. Helm, and H. Schmidt, J. Appl. Phys. **109**, 124117 (2011).
[5] S. H. Jo, K.-H. Kim, and W. Lu, Nano Lett. **9**, 870–874 (2009).
[6] E. Linn, R. Rosezin, C. Kügeler, and R. Waser, Nature Mater. **9**, 403–406 (2010).
[7] T. Driscoll, H.-T. Kim, B.-G. Chae, M. Di Ventra, and D. N. Basov, Appl. Phys. Lett. **95**, 043503 (2009).
[8] J. M. Tour and T. He, Nature (London) **453**, 42–43 (2008).
[9] Y. Ho, G. M. Huang, and P. Li, IEEE Trans. Circuits Syst. I **58**, 724–736 (2011).
[10] J. Rajendran, H. Manem, R. Karri, and G. S. Rose, IEEE Trans. Electron. Comput. **61**, 474–487 (2012).
[11] A. Ukil, IEEE Sens. J. **11**, 2514–2517 (2011).
[12] J. H. Song, Y. Zhang, C. Xu, W. Z. Wu, and Z. L. Wang, Nano Lett. **11**, 2829–2834 (2011).
[13] T. Driscoll, J. Quinn, S. Klein, H. T. Kim, B. J. Kim, Yu. V. Pershin, M. Di Ventra, and D. N. Basov, Appl. Phys. Lett. **97**, 093502 (2010).
[14] A. Chanthbouala, R. Matsumoto, J. Grollier, V. Cros, A. Anane, A. Fert, A. V. Khvalkovskiy, K. A. Zvezdin, K. Nishimura, Y. Nagamine, H. Maehara, K. Tsunekawa, A. Fukushima, and S. Yuasa, Nat. Phys. **7**, 626–630 (2011).
[15] D. Querlioz, O. Bichler, and C. Gamrat, in *Proceedings of the 2011 International Joint Conference on Neural Networks (IJCNN)* (IEEE, 2011), pp. 1775–1781.

This article is copyrighted as indicated in the article. Reuse of AIP content is subject to the terms at: http://scitationnew.aip.org/termsconditions. Downloaded to IP: 130.60.6.54 On: Tue, 13 May 2014 07:16:36